A Monte Carlo Method for Simulating Scattering From Sea Ice Using FVTD

Dustin Isleifson, *Member, IEEE*, Ian Jeffrey, *Member, IEEE*, Lotfollah Shafai, *Life Fellow, IEEE*, Joe LoVetri, *Senior Member, IEEE*, and David G. Barber

***Abstract*—A scattering model based on a Monte Carlo method and the finite-volume time-domain (FVTD) method has been created for sea ice scattering simulations. Statistical methods were used to generate a Gaussian-distributed randomly rough surface. The Polder–Van Santen–de Loor (PVD) model was used to estimate the sea ice dielectric values with inputs based upon actual measured physical variables obtained during field-based experiments and well-known parameterizations. Scattering simulations were performed through an application of the scattered-field (SF) formulation invoked in an FVTD computational engine. Simulated SFs were compared with C-band scatterometer measurements and showed good agreement for copolarized signals in a series of case studies. The developed simulation method has the potential to be used for a variety of sea ice types under different physical conditions.**

***Index Terms*—C-band, finite-difference time-domain (FDTD), finite-volume time domain (FVTD), scatterometer, sea ice.**

I. Introduction

THE ARCTIC cryosphere is a fragile environment that has received significant attention in the past decades due to the rising concern in climate change. General circulation models used to describe our planet's climate system have indicated that Arctic sea ice is highly sensitive to global climate change. Sea ice type and extent are inherently linked to the atmospheric and oceanic forcing mechanisms through the surface energy balance; moreover, there has been an observed dramatic depletion of sea ice in the Arctic over the past few decades [1]. Global climate change has major impacts not only in terms of direct changes to the environment but also on societal stability, transportation, and natural resource availability.

Microwave remote sensing has been used for many years to observe and assess the changes in the sea ice system in the Arctic [2]. The microwave scattering signatures of sea ice, at a given point in time and space, are dependent upon the time history of the evolution of the physical properties of the sea ice. Studies on the time series (i.e., seasonal evolution) of remote sensing data show that characteristic patterns exist, and therefore, microwave scattering signatures can be used to develop applications for deriving the state of the Arctic. Barber [2] has also suggested that remote sensing data can be fused into numerical climate models and can also be coupled to physical–biological models.

Microwave scattering signatures of sea ice can be studied directly through dedicated field campaigns and projects, while simultaneously, modeling studies can be undertaken to simulate the expected backscattering from a hypothetical sea ice medium. The scattering signatures of sea ice are governed by the surface roughness, the inhomogeneities within the ice, and the thermodynamic state of the ice [3]; therefore, in order to interpret the sea ice scattering signatures, a relationship between the electromagnetic behavior of the sea ice and the geophysical description must be determined [4]. The mechanisms under which the ice formed, how it has changed over time, and the age of the ice all are factors in determining the microwave properties and, therefore, the measured backscatter of the sea ice. Details on the characteristics of sea ice are well documented in the literature (see, for example, [5] and [6]). The thermodynamic and physical state of the sea ice medium should be considered in both dielectric and scattering models. Characterization of the geophysical parameters must be improved so that the associated models have a larger range of validity and so that we can better understand the limitations of the model [7]. Furthermore, it is important to test new modeling methods and techniques, as they may give new insight for problems that have been previously attempted. For example, polarimetric scattering signatures have the potential to give more information on the sea ice state since different polarizations may interact differently with components of the sea ice structure. Indeed, modern satellite-based synthetic aperture radar systems are polarimetric (e.g., Radarsat-2), so modeling efforts should be made to replicate the measurements.

Past research efforts have made great strides in our understanding of the mechanisms of electromagnetic wave interaction with the highly inhomogeneous sea ice medium. An excellent review of models used for microwave remote sensing has been provided in [8]. Examples of some past models that have been used for modeling sea ice remote sensing include models based on analytic wave theory (AWT) (Nghiem *et al.* [9]), with a part of the model based on strong fluctuation theory to calculate the effective permittivities (Stogryn [10]), radiative transfer theory (RT) (Ishimaru [11]), and dense medium radiative transfer theory. Surface scattering models have also been

Manuscript received June 4, 2011; revised October 13, 2011; accepted October 23, 2011. Date of publication December 7, 2011; date of current version June 20, 2012. The work of D. Isleifson was supported by a Natural Sciences and Engineering Research Council (NSERC) graduate scholarship, and that of L. Shafai and D. G. Barber was supported by NSERC operating grants and a Canada Research Chairs grant.

D. Isleifson, I. Jeffrey, L. Shafai, and J. LoVetri are with the Department of Electrical and Computer Engineering, University of Manitoba, Winnipeg, MB R3T 5V6, Canada (e-mail: disl@ee.umanitoba.ca; ijeffrey@ee.umanitoba.ca; shafai@ee.umanitoba.ca; joe_lovetri@umanitoba.ca).

D. G. Barber is with the Centre for Earth Observation Science and the Faculty of Environment, University of Manitoba, Winnipeg, MB R3T 2N2, Canada (e-mail: dbarber@cc.umanitoba.ca).

Digital Object Identifier 10.1109/TGRS.2011.2173940

applied under the geometric optics approximation, perturbation theory (for example, the small perturbation model (SPM) [12]), and integral equation methods (IEMs). As an alternative to the AWT and RT formulations, numerical computation methods have been used for simulating the interaction of waves with sea ice. While AWT formulations are generally quite complex, numerical simulation techniques can accommodate variations in complex media descriptions relatively easily. For example, Nassar studied the utility of FDTD for scattering from sea ice [13] and found that he was able to simulate scattering for midrange incidence angles with some success. Furthermore, fully developed simulation tools based on AWT and advanced RT models are not readily available, so considerable time in developing, debugging, and validating one of the models would be required.

Numerical techniques, such as the finite-volume time-domain (FVTD) method, have the potential to provide new information on sea ice scattering mechanisms. For example, the FVTD method uses an unstructured mesh, which provides a better physical representation of a rough surface than the cubic lattice of the FDTD method. While it is true that Monte Carlo techniques can be time consuming and require large computing resources, modern processors and parallelization of algorithms can mitigate some of the computational demands. Furthermore, FVTD is a time-domain method, which means that it is capable of providing scattering simulation results for a broad band of frequencies simultaneously.

In this paper, we describe a Monte Carlo method scattering model that uses the FVTD method and compare our simulations with actual measurements of sea ice obtained using a C-band scatterometer system. We show that our simulation technique matches the measurements for copolarized signals (i.e., σ^0_{HH}) in a series of case studies that have well-characterized ground-truth data (sea ice salinity, temperature, etc.). We focus on the validation of the numerical technique in our case studies, rather than specifically competing with other methods. In all cases, we are explicitly simulating undeformed young sea ice, meaning that ridges, rafting, and large-scale roughness are not considered in the present study.

II. Field Sampling Methods

We have conducted a large series of C-band scatterometer experiments from the Canadian Coast Guard Ship (CCGS) *Amundsen* as part of the Circumpolar Flaw Lead (CFL) System Study. High-quality geophysical characterizations of sea ice were performed after the region was interrogated using a ship-based scatterometer system. Portions of these data have been analyzed, for example, to understand the relationships between sea ice thickness and surface characteristics and the measured polarimetric backscattering response [14].

Upon arrival at a sea ice floe of interest, we guided the ship to a position that allowed the footprint of the scatterometer to illuminate as homogeneous ice surface as possible (i.e., with such thin ice, cracks and rafting of the ice were always present to some extent). We performed an average of five sets of scatterometer measurements to ensure that we had a statistically significant representation of the scattering properties of the area of interest. After the scatterometer measurements were complete, we visited the ice surface to obtain physical samples of the sea ice from within the scan region.

TABLE I
C-Band Scatterometer Operating Parameters [16]

Parameter	Value
Center Frequency	5.5 GHz
Bandwidth	500 MHz
Antenna Type	Parabolic Reflector
Antenna 3-dB Beamwidth	5.5°
Antenna Gain	28 dBi
Cross-polarization Isolation	>28 dB
Estimated Sensitivity	-40 dB
Transmit/Receive Polarizations	HH, VV, HV, VH

A. C-Band Scatterometer System

The C-band polarimetric scatterometer system was mounted on the port side of the icebreaker CCGS *Amundsen* at a height of about 8 m with respect to the sea surface. The system operates with a center frequency of 5.5 GHz and a bandwidth of 500 MHz. The antenna was a dual-polarized reflector with a beamwidth of approximately 5.5° in both the E-plane and H-plane. The system parameters are summarized in Table I. Measurements were conducted in 60° azimuth swaths over a 20° to 60° incidence angle range with a 5° increment. The returned power and phase information was measured, and the covariance matrix was calculated allowing σ^0_{VV}, σ^0_{VH}, and σ^0_{HH} normalized radar cross sections (NRCSs) and various polarimetric parameters to be obtained. Further details on the processing techniques are given in [14] and [15].

B. Physical Sampling Methods

The air temperature was measured by holding a hand-held temperature probe (Traceable Digital Thermometer, Control Company, accuracy ± 0.05 °C) approximately 1 m above the ice surface. Temperatures at the ice surface were taken by placing the probe in good contact with the surface and ensuring that the temperature had stabilized. When the ice was very thin (such as in our Case Study I), we directly measured the temperature of the ice–water interface by reaching into the water and pressing the probe against the bottom side of the ice. Generally, a representative core was extracted using an ice coring system (Mark II, Kovacs Enterprises), but for our Case Study I, we directly cut a section out of the ice using a handsaw. Ice temperatures were measured by inserting the temperature probe into a hole drilled into the center of the ice core or segment. A mean ice temperature was estimated by assuming a linear temperature profile. Ice thickness was measured from the extracted core or segment using a ruler, and we estimate our error to be ± 0.5 cm.

For salinity and texture analysis, extracted ice samples were placed in plastic bags and stored in a -20 °C freezer on the ship. Samples of the ice surface (i.e., scrapings of the top 2.5 mm) were taken for the salinity measurements. The ice cores were sliced into 5-cm segments (i.e., 5-cm tall cylinders) in the -20 °C cold laboratory on board the ship. The outer

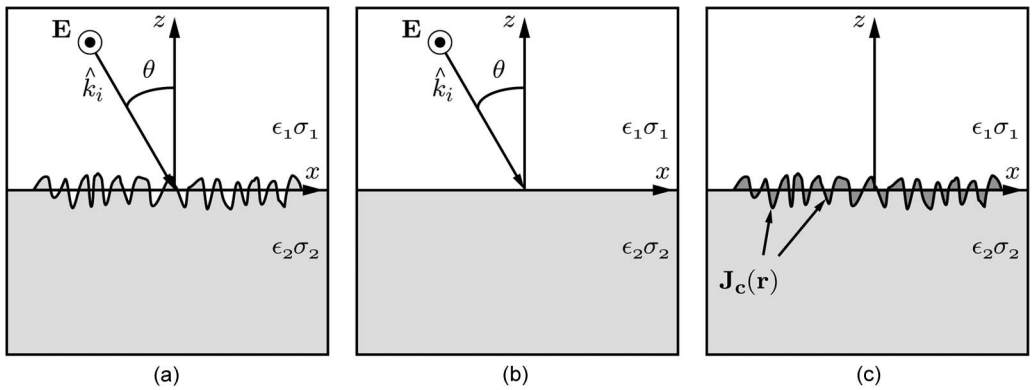

Fig. 1. Hypothetical geometry illustrating the decomposition of the fields in the SF formulation for the rough surface scattering problem. (a) Total-field geometry with the plane-wave source, **E**, incident upon a rough surface. (b) Incident-field geometry with only the dielectric half space and the plane-wave source. (c) SF geometry where the contrast sources $[\mathbf{J}_c(\mathbf{r})]$, which represent the rough surface undulations, radiate in the presence of the half-space background medium.

edges where the ice core had contacted the sea water were trimmed away in order to minimize the effects of the exposure. These samples were allowed to melt in plastic containers at room temperature, and the conductivity was measured with a conductivity meter (Hach Sens Ion 5). The salinities of the samples were calculated from the conductivity according to the formulation of [17], and a bulk salinity of the core was determined. More detailed descriptions of the physical sampling procedures are available elsewhere (e.g., [18]).

III. Monte Carlo Method for Rough Surface Scattering Simulations

In this section, we describe a Monte Carlo method for simulating electromagnetic scattering from an area-extensive target. As the primary measurement retrieved from the scatterometer system is the NRCS (symbolically denoted as σ^0), the output of our Monte Carlo simulation technique must therefore be the NRCS in order to facilitate comparison between simulation and measured results. The method uses the scattered-field (SF) formulation of an FVTD computational engine to propagate the fields through a geometry that represents a sea ice medium. The stochastic aspect of our Monte Carlo Method comes from the generation of many different realizations of a random rough surface. These realizations are generated to provide statistical variation for the simulated SFs. For each of these realizations, an approximate near-field to far-field transformation is used to calculate the far fields, and these are subsequently used to calculate the NRCS.

A Monte Carlo method for simulating scattering from sea ice using a combination of the FDTD and FVTD methods has the potential to provide new insight and information. Some of the advantages of the proposed technique include the following:

1) solves Maxwell's equations exactly, within numerical approximation;
2) can obtain broad-band results in one Monte Carlo run;
3) can add an unlimited number of layers to create a random media model;
4) can add random inclusions with relative ease;
5) can add surface roughness with relative ease;
6) can investigate other interesting features, such as cracks and rafting of sea ice.

At the same time, there are distinct disadvantages that the use of the FDTD–FVTD Monte Carlo model may encounter.

1) Proper spatial discretization of the sea ice medium restricts the size of the computational domain.
2) Monte Carlo techniques can be time consuming and require large computing resources.

For context, other researchers have applied the FDTD method to problems involving scattering objects in random media [19] and scattering from objects in stratified media [20]. Uchida [21] has reported on using the FVTD method for scattering from a randomly rough surface at grazing angles with application to communications and found that the results compared favorably with IEM methods. Still, other research has been performed that involves the analysis of heterogeneous rough media using FDTD [22]. There was a numerical study of electromagnetic scattering from sea ice using FDTD that is similar to our research [13]. To the best of our knowledge, no one has applied the FVTD method to modeling microwave remote sensing of sea ice.

A. FVTD Computations

The FVTD method is a differential-equation-based numerical scheme that is capable of simulating electromagnetic problems in three dimensions [23], [24]. In contrast to the FDTD method, the FVTD method can support an unstructured mesh, which has the capability to conform to irregular shapes and surfaces without requiring an extremely high level of discretization. In this paper, a parallel implementation of the FVTD algorithm is used. Pertinent details of the algorithm have been discussed in [24] and [25].

B. SF Formulation

In order to perform scattering simulations, we utilize a SF formulation, which is implemented using a combination of FDTD and FVTD techniques. Our method follows [26] and is described in [25].

The total-field geometry, which consists of a multilayered medium illuminated by a plane-wave source, is illustrated in Fig. 1(a). Using the standard SF decomposition, we separate the total-field simulation into an incident-field simulation [see Fig. 1(b)] and an SF simulation [see Fig. 1(c)]. We solve the

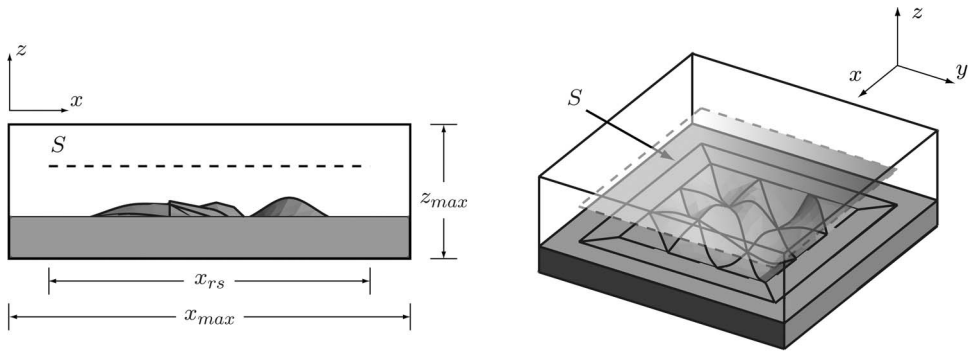

Fig. 2. Example of the mesh used in the rough surface scattering computations with the size of mesh elements enlarged for the sake of illustration. Left-hand figure shows a side view of the mesh and indicates the location of the integration surface S. Right-hand figure shows an isometric view of the rough surface mesh and also shows the location of the integration surface S with respect to the rough surface and the computational boundaries.

incident-field simulation first, which is the propagation of a plane wave through multilayered media. The solution is computed using a 1-D-FDTD solver. The solution to the incident-field simulation is subsequently used as the source for the SF simulation using FVTD. The SF geometry is shown in Fig. 1(c), where the contrast sources (i.e., $\mathbf{J}_c(\mathbf{r},t) \neq 0$) exist in regions where there is a difference in the electrical properties between the incident-field and the total-field geometries. The contrast sources can represent rough surface undulations. The SFs from these contrast sources propagate within the computational domain and are effectively absorbed by the absorbing boundary condition (ABC) at the edge of the domain. Further details on the methods are given in [25] and [27].

C. Rough Surface Generation

A computational geometry containing a layered medium and a rough surface must be constructed for the FVTD computations. An example of a rough surface computational geometry is given in Fig. 2. A randomly rough surface can be characterized by its autocovariance function (ACF) and its height distribution function (HDF). The ACF describes the lateral variation of distribution (associated with the correlation length L_c), while the HDF describes the height deviation from a mean value (denoted as σ_r). Commonly used ACFs include the Gaussian, 1.5-power, and the exponential [28]. We utilized a Gaussian distribution for our sea ice model since we did not have actual measurements of the surface roughness. To generate a rough surface, the method presented in [29] and originally given in [30] is employed. The surface is constructed from a $2D$ matrix of uncorrelated random points, $z_u = f(x,y)$, using a random number generator with a Gaussian distribution.

A Gaussian filter, given by

$$F(x,y) = \frac{2}{L_c\sqrt{\pi}} exp\left(-2(x^2+y^2)/L_c^2\right) \tag{1}$$

provides the means to obtain a correlation of the points through a convolution operation of the random points with the filter

$$z(x,y) = \int_{-\infty}^{\infty}\int_{-\infty}^{\infty} F(x-x',y-y')z_u(x',y')dx'dy'. \tag{2}$$

In practice, the convolution operation is performed using an inverse discrete Fourier transform (DFT).

D. Computation of NRCS

In order to calculate the NRCS σ^0 for a random surface, the statistical properties of the scattered power must be used. For an area-extensive target, σ^0 is computed as [31]

$$\sigma^0(\theta^{sc},\phi^{sc},\theta^{inc},\phi^{inc}) = \lim_{R\to\infty} 4\pi R^2 \frac{\langle S^{sc}(\theta^{sc},\phi^{sc})\rangle}{A_0 S^{inc}(\theta^{inc},\phi^{inc})} \tag{3}$$

where the superscript inc and sc denote incident and scattered quantities, A_0 is the area of illumination, $P^{inc} = A_0 S^{inc}(\theta^{inc},\phi^{inc})$ is the incident power, and $\langle . \rangle$ denotes ensemble averaging.

The SF from a random medium can be separated into coherent and incoherent components. The incoherent component is used to calculate the NRCS and is defined as

$$P^{incoherent} = \left\langle \left| E^c - E^n \right|^2 \right\rangle \tag{4}$$

where the superscript c and n represent the mean coherent field and the field from the nth Monte Carlo simulation, respectively.

When using our FVTD-based scattering model, we calculate the far fields in a postprocessing step, after the simulation has terminated (FVTD only computes fields within the computational domain). Field values are stored at discrete observation points on a fictitious surface, depicted as S in Fig. 2. We perform a DFT at each of the observation points and evaluate the convergence of the results at the completion of the simulation. After the FVTD simulation has terminated, a simple numerical integration is performed to calculate the radiation integrals. The near-field to far-field transformation is performed through an approximation to the surface equivalence theorem in electromagnetics [32].

Scattering from a limited region of a rough surface is analogous to radiation from an aperture in aperture theory. An effective area of illumination (depicted as S in Fig. 2) is created to represent an antenna footprint. Outside of the effective area of illumination, the contribution of the fields is considered to vanish (i.e., no contribution at all). Our hypothesis is that the rough surface itself can be tapered (i.e., it becomes smooth at the edges) in place of tapering the incident field.

As a test of concept, we have performed studies on the effects of the dimensions of $x_{\max}$ and x_{rs} on the simulated NRCS for a given statistical description and compared them to SPM results. For example, we generated $n = 20$ rough

surfaces with parameters $\sigma_r = 0.001$ m and $L_c = 0.005$ m for $x_{\max} = y_{\max} = 17$ cm and $x_{rs} = y_{rs} = 15$ cm and, again, for $x_{\max} = y_{\max} = 20$ cm and $x_{rs} = y_{rs} = 22$ cm. We found that the results of each of the Monte Carlo simulations agreed to within 2 dB of the SPM for all frequencies tested, which is acceptable considering the statistical nature of the problem.

Other researchers have chosen to use an illumination that has a Gaussian taper in the spatial domain [33], [34]. This ensures that the incident field does indeed vanish at the edges of the computational domain. The concept of a locally rough interface was proposed in [35] to model scattering sources above and below a planar interface, which is a similar idea to our proposed method. Additionally, in [36], it was warned that there could be pitfalls in using a plane wave to illuminate a finite rough surface since the ends of the surface could give large spikes in the surface current, but with the proposed method, we do not observe the spikes since our scatterers are effectively discrete objects.

We calculate the incident power upon the surface S by generating a computational geometry that is only free space. In this FVTD simulation, the incident field for layered media is therefore propagating only in free space and is not perturbed by any layered dielectric. The incident power can be calculated using the following integral, which is evaluated numerically on the same observation plane as the SF, and uses the time-harmonic values of the field quantities. This quantity must be calculated for each separate incidence angle

$$P^{inc} = \frac{1}{2} Re \left\{ \int_{y_1}^{y_2} \int_{x_1}^{x_2} \mathbf{E}^{inc} \times \mathbf{H}^{inc*} dx dy \right\} \tag{5}$$

where x_1 and x_2 are the bounds of the observation plane (i.e., S) in the x-dimension, y_1 and y_2 are the bounds of the observation plane in the y-dimension, $\mathbf{E}_{inc}$ and $\mathbf{H}^{inc*}$ are the time-harmonic incident-field values, and the $*$ denotes complex conjugation. The calculation of the incident power is required for normalization, as given in (3).

IV. Model Application and Comparison With Scatterometer Data

We have collected many scatterometer measurements, along with coincident geophysical measurements, during the CFL project. In this section, we present the results of a series of modeling case studies that were conducted to evaluate the applicability of the proposed Monte Carlo method for simulating electromagnetic scattering from sea ice using FVTD.

We presented a Monte Carlo method for simulating electromagnetic scattering from a rough surface in [27] and now apply this technique to model scattering from sea ice. Inherent with any statistical technique is the error associated with only a finite number of realizations. In our work, we have decided to use up to 24 different realizations to represent the sea ice medium. We chose a maximum of 24 realizations as a compromise between running a prohibitively large number of simulations and generating results with some statistical significance. A larger number of realizations would provide a lower error; moreover, the convergence of the results showed that the obtained values are adequate for the purposes of our modeling.

TABLE II
Literature Values for Sea Ice Surface Roughness Parameters for Newly Formed Sea Ice. The Acronym CRREL (EX) Refers to Experimental Work Performed at the U.S. Army Corps of Engineers Cold Regions Research and Engineering Laboratory

σ_r[m]	L_c[m]	Reference
0.0002-0.0048	0.00669-0.0177	CRREL'88 [28]
0.00216	0.0047	CRRELEX'90 [37]
0.00136	0.0176	CRRELEX'90 [37]
0.0005	0.0175	CRREL'94 [13]
0.0019	0.008	CRREL'94 [13]

Ideally, we would have liked to simulate a region that was the same size as the scatterometer footprint to represent the rough surface; however, 3-D FVTD simulations of regions greater than several wavelengths are computationally demanding (for $f = 5.5$ GHz and $\lambda_0 = 5.4545$ cm). In order to overcome this problem, we created a large number of smaller realizations that represented the sea ice medium in a Monte Carlo modeling study of the scattering properties. The scattering from one simulation of the sea ice medium provided a single sample of the scattering characteristics of this highly inhomogeneous medium.

In this modeling study, we made the assumption that all of the significant scattering interactions would take place at the surface of the sea ice since newly formed sea ice is generally a highly lossy dielectric material at microwave frequencies. We relied on literature values of surface roughness parameters for sea ice since we were not able to consistently and accurately measure the surface roughness in our fieldwork. Example literature values are given in Table II to provide a relative range of sea ice surface roughness parameters. Generally, we expect that the height variation σ_r should be on the order of millimeters, whereas the correlation length L_c should be on the order of centimeters. Note that, in Table II, the acronym CRREL(EX) refers to the experimental work performed at the U.S. Army Corps of Engineers Cold Regions Research and Engineering Laboratory.

The computational geometry was created using a freeware mesh-generating program, GMSH [42], which was also used to transform the physical description into a mesh for FVTD computations. The time function of the input waveform was a Gaussian derivative

$$E_y(t) = \frac{2A(t - t_0)}{b^2} exp\left(-(t - t_0)^2/b^2\right) \tag{6}$$

where $A = 1$, $t_0 = 0.2$ ns, and $b = 70$ ps. The constants in (6) were chosen such that sufficient energy would propagate at the frequency of interest (specifically, 5.5 GHz).

Estimations of dielectric properties of the sea ice medium were obtained through well-established dielectric modeling techniques. The models that we used are summarized in Table III, where we provide a list of input parameters, the associated model parameter, and a literature reference. Details of the usage of the models is given in each of our case studies. In our case studies, simulations were conducted only for the TE case, i.e., a horizontally polarized incident field. From our simulations, we obtain both the copolarized return σ^0_{HH} and the cross-polarized return σ^0_{VH}.

TABLE III
MODEL INPUT PARAMETERS AND CORRESPONDING REFERENCES

Input Parameter	Model Parameter	Literature Reference
f, T_{ice}	ϵ_{ice}	Mätzler *et al.* [38]
f, T_{ice}	ϵ_{brine}	Stogryn & Desargent [39]
T_{ice}, S_{ice}	v_b	Frankenstein & Garner [40]
$v_b, \epsilon_{ice}, \epsilon_{brine}$	ϵ_{seaice}	PVD, cited in [41]
Thickness	d_{ice}	Isleifson *et al.* [14]

TABLE IV
PHYSICAL PARAMETERS AND EVALUATED DIELECTRIC VALUES FOR CFL STATION 1800C

Thickness	d_{ice} = 5.5 cm
Ice Surface Temperature	T_{si} = -8.74°C
Mean Ice Temperature	T_{msi} = -5.21°C
Ice Bottom Temperature	T_{iw} = -1.68°C
Bulk Ice Salinity	S_b = 11.8 PSU
Brine Volume Fraction	v_b = 11.5%
Brine Dielectric	$\epsilon_{brine} = 50.0011 + j43.6265$
Pure Ice Dielectric	$\epsilon_{ice} = 3.1837 + j0.0010$
Sea Ice Dielectric	$\epsilon_{seaice} = 4.5241 + j0.2118$
Sea Ice Conductivity	$\sigma_{seaice} = 0.06480$

Since we did not have actual measurements of the surface roughness parameters, we used SPM to give us an initial guess for L_c and σ_r. We performed a series of simulations varying the surface roughness parameters and found values that provided good agreement between simulated and measured NRCSs in a manual optimization problem. We constrained our optimization problem by assuring that our surface roughness parameters were within the range of literature data (see Table II). In summary, we generated $n = 24$ realizations by prescribing roughness parameters and created a computational geometry for each realization. The same $n = 24$ realizations were used for simulations at each incidence angle (i.e., $20^\circ, 25^\circ, \ldots, 60^\circ$).

Furthermore, we optimized our simulations to obtain the best agreement for copolarized signals. We were not able to simultaneously optimize both the copolarized return σ^0_{HH} and the cross-polarized return σ^0_{VH}. This indicates that the model does not fully account for all relevant scattering behavior (for example, there is no attempt to simulate volumetric scattering).

A. Case Study I: CFL Station 1800C

We utilized the data collected at CFL Station 1800C as our first example of sea ice remote sensing. The sea ice at CFL Station 1800C was a newly formed sea ice type known as nilas, which exhibited an average thickness of 5.5 cm. From the microstructural analysis (not presented here but performed in a parallel ice physics study), it appeared to have formed under quiescent conditions. Physical measurements of the sea ice were conducted as described in Section II-B, and these data provide the baseline input for both our dielectric and scattering models. The relevant details of the physical and electrical data for this measurement location are summarized in Table IV. The mean ice temperature was calculated by averaging the ice surface and ice–water interface temperatures. The *in situ* temperature and laboratory calculated salinity were used to calculate brine volume according to Frankenstein and Garner [40].

TABLE V
FVTD SIMULATION PARAMETERS FOR CFL STATION 1800C

Modeling Domain Parameters	$x_{max} = y_{max}$ = 0.17 [m]
	$x_{rs} = y_{rs}$ = 0.15 [m]
	z-dimension = 0.025 [m]
	# of elements = 1.75 million
Rough Surface Parameters	σ_r = 0.00062
	L_c = 0.015

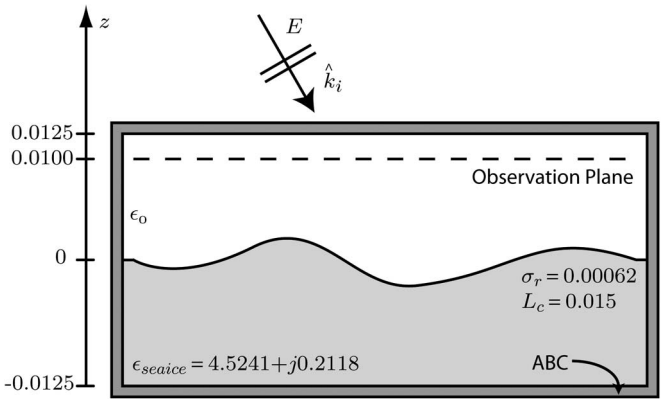

Fig. 3. Two-dimensional slice of the FVTD computational geometry for CFL station 1800C.

The brine volume fraction and *in situ* temperature were then used to calculate both the dielectric constant of the brine using the equations derived by Stogryn and Desargent in [39] and the dielectric constant of the ice using the expressions given by Mätzler *et al.* [38]. Finally, an estimate of the dielectric mixture was obtained using the Polder–Van Santen–de Loor (PVD) model assuming spherical brine pockets.

With the dielectric properties of the medium defined, the FVTD modeling domain was created next. The input parameters and some of the details on the computational domain are summarized in Table V. We set the dimensions as $x_{\max} = y_{\max} = 17$ cm and $x_{rs} = y_{rs} = 15$ cm (see Fig. 2). An illustration showing a 2-D slice of the geometry of the FVTD computational domain is shown in Fig. 3. The observation plane corresponds to the integration surface S.

The results of our simulations for σ^0_{HH} are presented in Fig. 4 and are compared with the scatterometer measurements. We have plotted the mean measured scatterometer results with the error bars showing the maximum and minimum measurement values of each scan. Our FVTD simulation results follow the trend of the scatterometer data reasonably well. At the incidence angles of 55° and 60°, the scatterometer measurements appear to saturate, i.e., they appear to reach a minimum value and do not decrease with increasing incidence angle. One possible explanation could be that there is a volumetric scattering aspect that is evident at these incidence angles, whereas it is not as dominant at the lower incidence angles [13]. Our FVTD simulations do not attempt to add a volumetric scattering element, so they continue to decrease with increasing incidence angle. Additionally, the effects of noise on the NRCS measured by the scatterometer could also be a source of error, in spite of our best efforts to ensure that the radar processing algorithm minimized its effects.

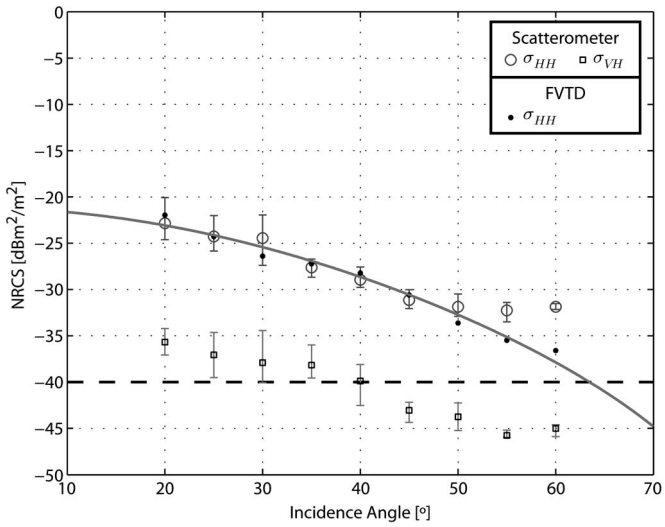

Fig. 4. Comparison of FVTD simulation results and scatterometer measurements at CFL Station 1800C. Solid line shows SPM results. The dashed line at -40 dB represents the estimated noise floor of the scatterometer.

The FVTD cross-polarized simulation results σ^0_{VH} are less than -50 dB (below the scatterometer noise floor) and are much lower than the scatterometer measurements. We conclude that our FVTD simulations have provided a good comparison with the scatterometer measurements for the copolarized signal σ^0_{HH}; however, the FVTD results have not replicated the results of the cross-polarized signal σ^0_{VH}.

In order to match the cross-polarized signal, we hypothesize that we would have to include some form of anisotropy for the sea ice dielectrics and/or the rough surfaces. The current implementation of the FVTD engine supports only isotropic media. As part of our future research, we could consider adding the capability for simulating anisotropic dielectric media in the FVTD engine in order to see its effects. Additionally, we could also consider using different surface roughness parameterizations. In all of our examples, we make the assumption that the rough surface follows a statistical distribution that is independent of direction. Although the sea ice in our parametric studies appeared to have grown under quiescent conditions, environmental effects (wind direction and wave action) could potentially impact the surface. By adding anisotropic capabilities, we could improve upon our physical description of the sea ice in the model and likely improve the match between our simulated and measured cross-polarized signals.

For comparison, in his model with ellipsoidal inclusions, Nghiem *et al.* [43] showed that, by simulating volume scattering alone, he could obtain good agreement between measured and simulated cross-polarized results. He notes that low surface roughness was a requirement such that cross-polarized scattering generated from the rough interface was negligible. In his example of scattering from thin lead ice (similar to our Case Study III: D28A), he shows that the cross-polarized signal is about 12 dB below the copolarized signal, for both simulation and measurement. This difference is comparable to our simulation and measurement results, which indicates that a similar assumption in our simulation could also be valid.

TABLE VI
PHYSICAL PARAMETERS AND EVALUATED DIELECTRIC VALUES FOR CFL STATION 1800B

Thickness	d_{ice} = 9 cm
Ice Surface Temperature	T_{si} = -10.7°C
Mean Ice Temperature	T_{msi} = -6.21°C
Bulk Ice Salinity	S_b = 13.7 PSU
Brine Volume Fraction	v_b = 11.4%
Brine Dielectric	$\epsilon_{brine} = 47.9030 + j44.0821$
Pure Ice Dielectric	$\epsilon_{ice} = 3.1827 + j0.0010$
Sea Ice Dielectric	$\epsilon_{seaice} = 4.5056 + j0.2183$
Sea Ice Conductivity	$\sigma_{seaice} = 0.0668$

TABLE VII
FVTD SIMULATION PARAMETERS FOR CFL STATION 1800B

Modeling Domain Parameters	x-dimension = 0.17 [m]
	y-dimension = 0.17 [m]
	z-dimension = 0.035 [m]
	# of elements = 1.7 million
Rough Surface Parameters	σ_r = 0.003027
	L_c = 0.018056

B. Case Study II: CFL Station 1800B

We utilized the data collected at CFL Station 1800B as our second example of sea ice remote sensing. The sea ice at CFL Station 1800B consisted of a sea ice type known as light nilas, with an average thickness of 9 cm. There were a few small frost flowers (< 1 cm) that populated the surface, and we estimated the percentage coverage as a maximum of 25%. We considered the frost flowers as a roughening of the surface, so the roughness parameters of this station are greater than that of Case Study I: CFL Station 1800C. The details of the physical and electrical data for this measurement location are summarized in Table VI.

With the dielectric properties of the medium defined, the FVTD modeling domain was created. The input parameters and some of the details on the computational domain are summarized in Table VII. In Table VII, the total z-dimension is a summation of the modeled sea ice layer and an overlying free-space layer. Again, we began the modeling process by considering the scatterometer measurements of the ice to be dominated by surface scattering. By varying the parameters of the surface roughness characterization, we found that we could match the scatterometer measurements almost perfectly by the correct choice. The values selected for the surface roughness characterization were within an acceptable range for newly formed sea ice (see Table II). A 2-D slice illustrating the geometry of the FVTD computational domain is shown in Fig. 5.

Although the thickness of the sea ice is 9 cm, we only modeled the top portion of the sea ice for three reasons. First, the exploration depth of the interrogating electromagnetic wave (using ϵ_{seaice}) is smaller than the complete ice thickness, so the bottom interface would play a minor role in the backscattering simulation. In other words, we hypothesize that this highly saline ice would present a predominantly surface scattering situation. Second, it would take considerably more time to

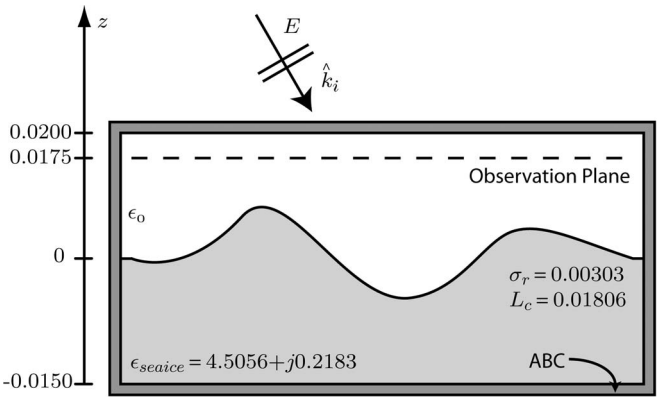

Fig. 5. Two-dimensional slice of the FVTD computational geometry for CFL station 1800B.

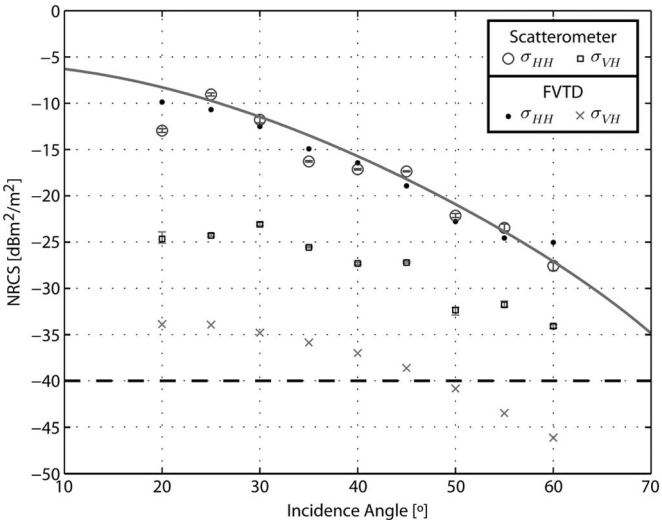

Fig. 6. Comparison of FVTD simulation results and scatterometer measurements at CFL Station 1800B. Solid line shows the SPM results. The dashed line at -40 dB represents the estimated noise floor of the scatterometer.

simulate a larger domain using our present method. Since the expected contribution from the ice–water interface is very small, it is inefficient to simulate the complete ice thickness. Third, we are approximating the sea ice as a homogeneous slab of constant dielectric, so the ABCs should effectively terminate the wave propagation with minimal reflection back into the solution domain. From a computational perspective, the sea ice appears to continue to negative infinity in the z-direction, so there would be no difference in simulating thicker sea ice (unless, of course, we went as far as to include the ice–water interface). Therefore, we only modeled the top 2 cm of the sea ice.

The results of our simulations for σ^0_{HH} and σ^0_{VH} are presented in Fig. 6 and are compared with the scatterometer measurements. We have plotted the mean measured scatterometer results with the error bars showing the maximum and minimum measurement values of each scan. Our FVTD simulation results follow the trend of the scatterometer data reasonably well for σ^0_{HH}; however, the FVTD simulations have not replicated the results of the cross-polarized signal σ^0_{VH}. This is likely due to limitations in the computational method; more specifically, we have assumed that the dielectric medium is completely isotropic and the rough surface is isotropic. It is not surprising that the simulated cross-polarized signal is lower than the measured cross-polarized signal since we have not taken all of the depolarizing factors into account in our model. Accounting for these features should be addressed in future work.

TABLE VIII
PHYSICAL PARAMETERS AND EVALUATED DIELECTRIC VALUES FOR CFL STATION D28A

Thickness	d_{ice} = 9 cm
Ice Surface Temperature	T_{si} = -12.6°C
Mean Ice Temperature	T_{msi} = -10.455°C
Bulk Ice Salinity	S_b = 17.1 PSU
Brine Volume Fraction	v_b = 9.2%
Ice Surface Salinity	S_{si} = 82.0 PSU
Slush Thickness	1 mm
Dielectric Values	(Slushy Layer)
Brine Dielectric	$\epsilon_{brine} = 37.5798 + j42.5864$
Pure Ice Dielectric	$\epsilon_{ice} = 3.1769 + j0.0010$
Slush Dielectric	$\epsilon_{slush} = 7.2173 + j1.7059$
Sea Ice Conductivity	$\sigma_{slush} = 0.52196$
Dielectric Values	(Sea Ice Layer)
Brine Dielectric	$\epsilon_{brine} = 40.5769 + j43.7644$
Pure Ice Dielectric	$\epsilon_{ice} = 3.1789 + j0.0010$
Sea Ice Dielectric	$\epsilon_{seaice} = 4.1711 + j0.1726$
Sea Ice Conductivity	$\sigma_{seaice} = 0.052811$

TABLE IX
FVTD SIMULATION PARAMETERS FOR CFL STATION D28A

Modeling Domain Parameters	x-dimension = 0.17 [m]
	y-dimension = 0.17 [m]
	z-dimension = 0.0325 [m]
	# of elements = 2.3 million
Rough Surface Parameters	σ_r = 0.00152649
	L_c = 0.0140625

C. Case Study III: CFL Station D28A

We utilized the data collected at CFL Station D28A as our third example of sea ice remote sensing. The sea ice at CFL Station D28A was newly formed lead ice with a thickness of 9 cm. The details of the physical and electrical data for this measurement location are summarized in Table VIII. This station was different from the previous two examples, particularly because it had a slushy layer that was around 1 mm in depth on the surface. In our modeling, we followed the approach of Nghiem *et al.* [44] who estimated that the slushy layer was 25% brine and 75% ice in a similar situation. We estimated the dielectric of this slushy layer by using the PVD model, under the assumption that the layer was a two-phase mixture of brine and ice, where the brine could be represented by spherical pockets.

With the dielectric properties of the medium defined, the FVTD modeling domain was created next. The input parameters and some of the details on the computational domain are summarized in Table IX. Again, we began the modeling process by considering the scatterometer measurements of the sea ice to be dominated by surface scattering. By varying the parameters of the surface roughness characterization, we found that we could match the scatterometer measurements almost perfectly

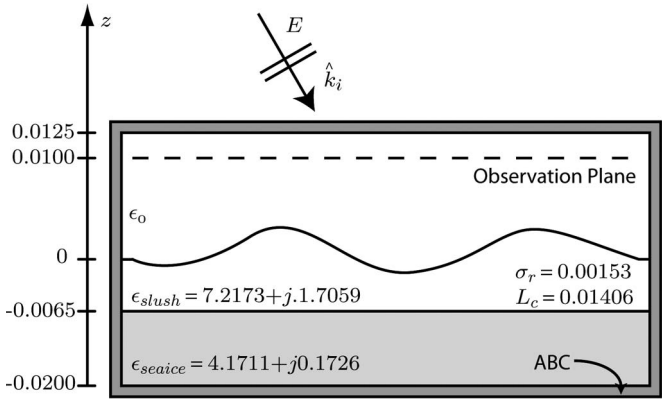

Fig. 7. Two-dimensional slice of the FVTD computational geometry for CFL station D28A.

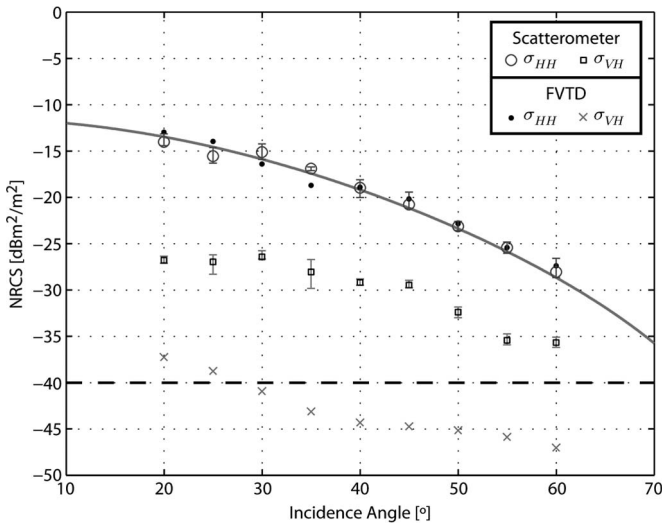

Fig. 8. Comparison of FVTD simulation results and scatterometer measurements at CFL Station D28A. Solid line shows SPM results. The dashed line at −40 dB represents the estimated noise floor of the scatterometer.

by the correct choice. The values selected for the surface roughness characterization were within an acceptable range of literature values. A 2-D slice of the geometry of the FVTD computational domain is shown in Fig. 7. The computational domain of CFL Station D28A consists of three layers (air, slush, and sea ice), as opposed to the previous two case studies, which consisted of two layers (air and sea ice).

The results of our simulations for σ^0_{HH} are presented in Fig. 8 and were compared with the scatterometer measurements. We have plotted the mean measured scatterometer results with the error bars showing the maximum and minimum measurement values of each scan. Our FVTD simulation results follow the trend of the scatterometer data reasonably well. We conclude that our FVTD simulations have provided a good comparison with the scatterometer measurements for the copolarized signal σ^0_{HH}; however, the FVTD simulations have not replicated the results of the cross-polarized signal σ^0_{VH}. Again, this is likely due to limitations in the computational method, where we have assumed that the dielectric medium is completely isotropic and the rough surface is isotropic. By adding more of the depolarizing features into our model, we hypothesize that we could improve the agreement between the simulated and measured cross-polarized signals.

V. Conclusion

This paper has combined the physical measurements of sea ice with dielectric modeling techniques for use in the FVTD remote sensing scattering model that we have developed. Several examples were given to show the applicability of the model, and we gave some discussion regarding the modeling issues that we have discovered. We have shown how our modeling technique can provide good agreement with field results for a variety of physical situations, even with approximations and estimations on the dielectric values and roughness scales. We have shown that the surface roughness parameters are a critical measurement, since we were able to achieve a reasonable match between simulated and measured results through a manual optimization of the roughness parameters. It is clear that the modeling method does not take all necessary aspects into account, since the measured and the simulated cross-polarized signal were not in good agreement and we were not able to simultaneously match both σ^0_{HH} and σ^0_{VH}.

We presented case studies that demonstrate the capability of the proposed FVTD-based Monte Carlo method for simulating the scattering from newly formed sea ice. These case studies were selected to provide a baseline comparison with other simple methods (e.g., SPM) and are not an attempt to compete with such methods. The range of roughness scale that we can simulate using the FVTD method is likely to be governed by the limitations of the computing facilities and user needs (i.e., how much memory we are willing to use and how long we are willing to wait for simulation results). The proposed method does not have the same restrictions on roughness ranges (such as SPM), so it may have a wider range of applicability. Additionally, although we have not demonstrated the capability in this work, the FVTD method has the ability to account for volumetric scattering by appropriate introduction of inhomogeneities into the computational geometry.

In our simulated copolarized results, the backscatter decreases monotonically with increasing incident angle. This is expected from the formulation of the problem. However, the measurements do not follow that same trend exactly, for example, in Case I: CFL Station 1800C, the backscatter at 30° is the same as that at 25°. In modeling, we make the assumption that the surface properties exhibit perfect horizontal homogeneity. Our field-based observations indicate that natural sea ice always has some horizontal variation.

We would like to point out (as Fung did in [28]) that many different models could potentially provide decent agreement with scatterometer measurements using different assumptions. It is only when the electrical parameters are modeled correctly and the scattering model takes into account all necessary interactions that we can expect that the model will give the "correct" result. This work is a step toward a fully polarimetric model.

Acknowledgment

The authors would like to thank V. Okhmatovski for the use of his computing cluster.

REFERENCES

[1] J. C. Comiso, C. L. Parkinson, R. Gersten, and L. Stock, "Accelerated decline in the Arctic sea ice cover," *Geophys. Res. Lett.*, vol. 35, p. L01 703, 2008.

[2] D. G. Barber, "Microwave remote sensing, sea ice and Arctic climate," *Phys. Can.*, vol. 61, pp. 105–111, 2005.

[3] W. B. I. Tucker, D. K. Perovich, A. J. Gow, W. F. Weeks, and M. R. Drinkwater, "Physical properties of sea ice relevant to remote sensing," in *Microwave Remote Sensing of Sea Ice*, vol. 68. Washington, DC: AGU, 1992, ch. 2.

[4] S. V. Nghiem, R. Kwok, S. H. Yueh, and M. R. Drinkwater, "Polarimetric signatures of sea ice 1. Theoretical model," *J. Geophys. Res.*, vol. 100, no. C7, pp. 13 665–13 679, Jul. 1995.

[5] W. F. Weeks and S. F. Ackley, The growth, structure, and properties of sea ice, CRREL, CRREL Monogr. 82-1, Hanover, NH, 1982.

[6] G. F. N. Cox and W. Weeks, "Profile properties of undeformed first-year sea ice," CRREL, Hanover, NH, 1988, Tech. Rep.

[7] D. P. Winebrenner, J. Bredow, A. K. Fung, M. R. Drinkwater, S. V. Nghiem, A. J. Gow, D. K. Perovich, T. C. Grenfell, H. C. Han, J. A. Kong, J. K. Lee, S. Mudaliar, R. G. Onstott, L. Tsang, and R. D. West, "Microwave sea ice signature modeling," in *Microwave Remote Sensing of Sea Ice*, vol. 68. Washington, DC: AGU, 1992, ch. 8.

[8] K. C. Jezek, D. K. Perovich, K. M. Golden, C. Luther, D. G. Barber, P. Gogineni, T. C. Grenfell, A. K. Jordan, C. D. Mobley, S. V. Nghiem, and R. G. Onstott, "A broad spectral, interdisciplinary investigation of the electromagnetic properties of sea ice," *IEEE Trans. Geosci. Remote Sens.*, vol. 36, no. 5, pp. 1633–1641, Sep. 1998.

[9] S. V. Nghiem, M. Borgeaud, J. A. Kong, and R. T. Shin, "Polarimetric remote sensing of geophysical media with layer random medium model," *Prog. Electromagn. Res. (PIER)*, vol. 3, pp. 1–69, 1991.

[10] A. Stogryn, "Strong fluctuation theory for moist granular media," *IEEE Trans. Geosci. Remote Sens.*, vol. GE-23, no. 2, pp. 78–83, 1985.

[11] A. Ishimaru, *Wave Propagation and Scattering in Random Media*, vol. 1/2. New York: Academic, 1978.

[12] S. O. Rice (1951, Aug.). Reflection of electromagnetic waves from slightly rough surfaces. *Commun. Pure Appl. Math.* [Online]. *4(2/3)*, pp. 351–378. Available: http://dx.doi.org/10.1002/cpa.3160040206

[13] E. Nassar, "Numerical and experimental studies of electromagnetic scattering from sea ice," Ph.D. dissertation, Ohio State Univ., Columbus, OH, 1997.

[14] D. Isleifson, B. Hwang, D. G. Barber, R. K. Scharien, and L. Shafai, "C-band polarimetric backscattering signatures of newly formed sea ice during fall freeze-up," *IEEE Trans. Geosci. Remote Sens.*, vol. 48, no. 8, pp. 3256–3267, Aug. 2010.

[15] T. Geldsetzer, J. Mead, J. Yackel, R. Scharien, and S. Howell, "Surface-based polarimetric C-band scatterometer for field measurements of sea ice," *IEEE Trans. Geosci. Remote Sens.*, vol. 45, no. 11, pp. 3405–3416, Nov. 2007.

[16] D. Isleifson, A. Langlois, D. Barber, and L. Shafai, "C-band scatterometer measurements of multiyear sea ice before fall freeze-up in the Canadian Arctic," *IEEE Trans. Geosci. Remote Sens.*, vol. 47, no. 6, pp. 1651–1661, Jun. 2009.

[17] N. P. Fofonoff, "Physical properties of seawater: A new salinity scale and equation of state for seawater," *J. Geophys. Res.*, vol. 90, no. C2, pp. 3332–3342, 1985.

[18] J. K. Ehn, B. J. Hwang, R. J. Galley, and D. G. Barber, "Investigations of newly formed sea ice in the Cape Bathurst polynya: 1. Structural, physical, and optical properties," *J. Geophys. Res.*, vol. 112, no. C5, p. C05 003, May 2007.

[19] C. D. Moss, F. L. Teixeira, Y. E. Yang, and J. A. Kong, "Finite-difference time-domain simulation of scattering from objects in continuous random media," *IEEE Trans. Geosci. Remote Sens.*, vol. 40, no. 1, pp. 178–186, Jan. 2002.

[20] K. Demarest, R. Plumb, and Z. Huang, "FDTD modeling of scatterers in stratified media," *IEEE Trans. Antennas Propag.*, vol. 43, no. 10, pp. 1164–1168, Oct. 1995.

[21] K. Uchida, K. Y. Yoon, and A. Ishimaru, "FVTD analysis of electromagnetic wave scattering by rough surface," in *Proc. IGARSS*, 1998, vol. IV, pp. 2292–2294.

[22] H. Chanal, J. P. Segaud, P. Borderies, and M. Saillard, "Homogenization and scattering from heterogeneous media based on finite-difference-time-domain Monte Carlo computations," *J. Opt. Soc. Amer. A, Opt. Image Sci.*, vol. 23, no. 2, pp. 370–381, Feb. 2006.

[23] P. Bonnet, X. Ferrieres, P. L. Michielsen, and P. Klotz, "Finite volume time domain method," in *Time Domain Electromagnetics*, S. M. Rao, Ed. San Diego, CA: Academic, 1999.

[24] D. Firsov, J. LoVetri, I. Jeffrey, V. Okhmatovski, C. Gilmore, and W. Chamma, "High-order FVTD on unstructured grids using an object-oriented computational engine," *ACES*, vol. 22, no. 1, pp. 71–82, 2007.

[25] D. Isleifson, I. Jeffrey, L. Shafai, J. LoVetri, and D. G. Barber, "An efficient scattered-field formulation for objects in layered media using the FVTD method," *IEEE Trans. Antennas Propag.*, vol. 59, no. 11, pp. 4162–4170, Nov. 2011.

[26] I. Capoglu and G. Smith, "A total-field/scattered-field plane-wave source for the FDTD analysis of layered media," *IEEE Trans. Antennas Propag.*, vol. 56, no. 1, pp. 158–169, Jan. 2008.

[27] D. Isleifson, L. Shafai, and D. G. Barber, "Numerical scattering from 3D randomly rough surfaces using FVTD," in *Proc. IEEE Int. Symp. Antennas Propag. USNC-URSI Nat. Radio Sci. Meeting*, 2011, pp. 3225–3228.

[28] A. K. Fung, *Microwave Scattering and Emission Models and Their Applications*. Norwood, MA: Artech House, 1994.

[29] D. Bergström, J. Powell, and A. F. Kaplan (2008, May). The absorption of light by rough metal surfaces—A three-dimensional ray-tracing analysis. *J. Appl. Phys.* [Online]. *103(10)*, p. 103 515. Available: http://link.aip.org/link/?JAP/103/103515/1

[30] N. Garcia and E. Stoll, "Monte Carlo calculation for electromagnetic-wave scattering from random rough surfaces," *Phys. Rev. Lett.*, vol. 52, no. 20, pp. 1798–1801, May 1984.

[31] L. Tsang and J. A. Kong, *Scattering of Electromagnetic Waves*. New York: Wiley, 2000.

[32] C. A. Balanis, *Advanced Engineering Electromagnetics*. New York: Wiley, 1989.

[33] A. K. Fung, M. R. Shah, and S. Tjuatja, "Numerical simulation of scattering from three-dimensional randomly rough surfaces," *IEEE Trans. Geosci. Remote Sens.*, vol. 32, no. 5, pp. 986–994, Sep. 1994.

[34] F. D. Hastings, J. B. Schneider, and S. L. Broschat, "A Monte Carlo FDTD technique for rough surface scattering," *IEEE Trans. Antennas Propag.*, vol. 43, no. 11, pp. 1183–1191, Nov. 1995.

[35] Y. Altuncu, A. Yapar, and I. Akduman, "On the scattering of electromagnetic waves by bodies buried in a half-space with locally rough interface," *IEEE Trans. Geosci. Remote Sens.*, vol. 44, no. 6, pp. 1435–1443, Jun. 2006.

[36] R. Marchand and G. Brown, "On the use of finite surfaces in the numerical prediction of rough surface scattering," *IEEE Trans. Antennas Propag.*, vol. 47, no. 4, pp. 600–604, Apr. 1999.

[37] S. G. Beaven, S. P. Gogineni, A. Gow, A. Lohanick, and K. Jezek, "Radar backscatter measurements from simulated sea ice during CR-RELEX'90," Inf. Telecommun. Technol. Center, Univ. Kansas, Lawrence, KS, RSL Tech. Rep. 8243-2, 1993.

[38] C. Mätzler and U. Wegmuller, "Dielectric properties of fresh-water ice at microwave frequencies," *J. Phys. D, Appl. Phys.*, vol. 20, no. 12, pp. 1623–1630, Dec. 1987.

[39] A. Stogryn and G. D. Desargant, "The dielectric properties of brine in sea ice at microwave frequencies," *IEEE Trans. Antennas Propag.*, vol. AP-33, no. 5, pp. 523–532, May 1985.

[40] G. Frankenstein and R. Garner, "Equations for determining the brine volume of sea ice from -0.5°C to -22.9°C," *J. Glaciol.*, vol. 6, no. 48, pp. 943–944, 1967.

[41] F. T. Ulaby, R. K. Moore, and A. K. Fung, *Microwave Remote Sensing: Active and Passive*, vol. 3. Norwood, MA: Artech House, 1986.

[42] C. Geuzaine and J.-F. Remacle, "Gmsh: A three-dimensional finite element mesh generator with built-in pre- and post-processing facilities," *Int. J. Numer. Methods Eng.*, vol. 79, no. 11, pp. 1309–1331, Sep. 2009.

[43] S. V. Nghiem, R. Kwok, S. H. Yueh, A. J. Gow, D. K. Perovich, J. A. Kong, and C. C. Hsu, "Evolution in polarimetric signatures of thin saline ice under constant growth," *Radio Sci.*, vol. 32, no. 1, pp. 127–151, 1997.

[44] S. V. Nghiem, R. Kwok, S. H. Yueh, and M. R. Drinkwater, "Polarimetric signatures of sea ice 2. Experimental observations," *J. Geophys. Res.*, vol. 100, no. C7, pp. 13 681–13 698, Jul. 1995.

Dustin Isleifson (M'11) received the B.Sc. degree in electrical engineering (with distinction) and the Ph.D. degree in electrical and computer engineering from the University of Manitoba, Winnipeg, MB, Canada, in 2005 and 2011, respectively.

He has conducted research in the Canadian Arctic through ArcticNet and the Circumpolar Flaw Lead System Study. He held a Canadian Natural Sciences and Engineering Research Council (NSERC) Canada Graduate Scholarship CGS-M in 2006 and held an NSERC Canada Graduate Scholarship CGS-D3 during his Ph.D. studies. He is currently a Postdoctoral Research Fellow with the Department of Electrical and Computer Engineering and the Centre for Earth Observation Science, University of Manitoba. His current research interests are in the areas of microwave remote sensing, computational electromagnetics, and Arctic science.

Ian Jeffrey (M'11) received the B.S. degree in computer engineering (with distinction) and the M.S. and Ph.D. degrees in electrical and computer engineering from the University of Manitoba, Winnipeg, MB, Canada, in 2002, 2004, and 2011, respectively.

In 2008, he was an intern at Cadence Design Systems, Inc., Tempe, AZ, where he worked with the Department of Custom Integrated Circuits Advanced Research and Development. He currently holds a Mathematics of Information Technology and Complex Systems industrial postdoctoral fellowship with the National Research Council Canada's Institute for Biodiagnostics. His current research interests include finite-volume and discontinuous Galerkin time-domain methods, fast algorithms for computational electromagnetics, high-performance computing, and inverse problems.

Lotfollah Shafai (F'87–LF'07) received the B.Sc. degree from the University of Tehran, Tehran, Iran, in 1963, and the M.Sc. and Ph.D. degrees in electrical engineering from the Faculty of Applied Sciences and Engineering, University of Toronto, Toronto, ON, Canada, in 1966 and 1969, respectively.

In November 1969, he joined the Department of Electrical and Computer Engineering, University of Manitoba, Winnipeg, MB, Canada, as a Sessional Lecturer, where he became an Assistant Professor in 1970, an Associate Professor in 1973, and a Professor in 1979. Since 1975, he has made special effort to link the university research to the industrial development, by assisting industries in the development of new products or establishing new technologies. To enhance the University of Manitoba contact with industry, in 1985, he assisted in establishing "The Institute for Technology Development" and was its Director until 1987, when he became the Head of the Electrical Engineering Department. His assistance to industry was instrumental in establishing an Industrial Research Chair in Applied Electromagnetics at the University of Manitoba in 1989, which he held until July 1994.

Dr. Shafai was elected a Fellow of The Royal Society of Canada in 1998. In 2002, he was elected a Fellow of The Canadian Academy of Engineering and Distinguished Professor at the University of Manitoba. He holds a Canada Research Chair in Applied Electromagnetics and was the International Chair of Commission B of the International Union of Radio Science (URSI) for 2005–2008. In 2009, he was elected a Fellow of the Engineering Institute of Canada. He has been a participant in nearly all antennas and propagation symposia and participates in the review committees. He is a member of URSI Commission B and was its Chairman during 1985–1988. In 1986, he established the Symposium on Antenna Technology and Applied Electromagnetics at the University of Manitoba that is currently held every two years. He has been the recipient of numerous awards. In 1978, his contribution to the design of a small ground station for the Hermus satellite was selected as the 3rd Meritorious Industrial Design. He was the recipient of the Professional Engineers Merit Award in 1984 and "The Thinker" Award from Canadian Patents and Development Corporation in 1985. From the University of Manitoba, he received the "Research Awards" in 1983, 1987, and 1989, the Outreach Award in 1987, and the Sigma Xi Senior Scientist Award in 1989. He was the recipient of the Maxwell Premium Award from IEE (London) in 1990 and the Distinguished Achievement Awards from Corporate Higher Education Forum in 1993 and 1994. In 1998, he received the Winnipeg RH Institute Foundation Medal for Excellence in Research. In 1999 and 2000, he was the recipient of the University of Manitoba Faculty Association Research Award. He was a recipient of the IEEE Third Millennium Medal in 2000. In 2003, he received an IEEE Canada "Reginald A. Fessenden Medal" for "Outstanding Contributions to Telecommunications and Satellite Communications" and a Natural Sciences and Engineering Research Council Synergy Award for "Development of Advanced Satellite and Wireless Antennas." In 2009, he was the recipient of an IEEE Chen-To-Tai Distinguished Educator Award. In 2011, he received a Killam Prize in Engineering from The Canada Council for the Arts for his "outstanding Canadian career achievements in engineering and his work in antenna research."

Joe LoVetri (SM'09) received the B.Sc. (with distinction) and M.Sc. degrees in electrical engineering from the University of Manitoba, Winnipeg, MB, Canada, in 1984 and 1987, respectively, the Ph.D. degree in electrical engineering from the University of Ottawa, Ottawa, ON, Canada, in 1991, and the M.A. degree in philosophy from the University of Manitoba in 2006.

From 1984 to 1986, he was an Electromagnetic Interference/Electromagnetic Compatibility Engineer at the Sperry Defence Division in Winnipeg, and from 1986 to 1988, he held the position of TEMPEST Engineer at the Communications Security Establishment, Ottawa, ON, Canada. From 1988 to 1991, he was a Research Officer at the Institute for Information Technology of the National Research Council of Canada. His academic career began in 1991 when he joined the Department of Electrical and Computer Engineering at the University of Western Ontario, London, ON, Canada, where he remained until 1999. In 1997–1998, he spent a sabbatical year at the TNO Physics and Electronics Laboratory in The Netherlands, doing research in time-domain computational methods and ground-penetrating RADAR. In 1999, he joined the University of Manitoba, where he is currently a Professor with the Department of Electrical and Computer Engineering. From 2004 to 2009, he was the Associate Dean (Research and Graduate Programs) for the Faculty of Engineering. His main research interests lie in the areas of time-domain computational electromagnetics, modeling of electromagnetic compatibility problems, inverse problems, and biomedical imaging.

David G. Barber received the B.S. and M.S. degrees from the University of Manitoba, Winnipeg, MB, Canada, in 1981 and 1987, respectively, and the Ph.D. degree from the University of Waterloo, London, ON, Canada, in 1992.

He is a Professor of environment and geography and Canada Research Chair in Arctic System Science in the Clayton H. Riddell Faculty of Environment Earth and Resources, University of Manitoba. He was appointed to a faculty position at the University of Manitoba in 1993 and received a Canada Research Chair in Arctic System Science in 2002. He is currently the Director of the Centre for Earth Observation Science and Associate Dean (Research) of the Clayton H. Riddell Faculty of Environment, Earth and Resources. He has extensive experience in the examination of the Arctic marine environment as a "system" and the effect that climate change has on this system. He led the largest International Polar Year (IPY) project in the world, known as the Circumpolar Flaw Lead (CFL) system study. He is recognized internationally through scientific leadership in large network programs (e.g., North Open Water Polynya, Canadian Arctic Shelf Exchange Study, ArcticNet, the Canadian Research Icebreaker (Amundsen), and CFL), as an invited member of several Natural Sciences and Engineering Research Council (NSERC) national committees (e.g., NSERC International Polar Year, NSERC northern supplements, etc.), international committees (Global Energy and Water Cycle Experiment, International Arctic Polynya Program, Canadian National Committee—Scientific Committee on Oceanic Research, International Arctic Research Center, etc.), and invitations to national and international science meetings (e.g., American Geophysical Union, Canadian Meteorological and Oceanographic Society, American Meteorological Society, American Society for Limnology and Oceanography (Spain), IMPACTS (Russia), European Space Agency (Italy), Arctic Frontiers (Norway), etc.). He currently supervises nine M.Sc. students, nine Ph.D. students, four postdoctoral fellows, and nine full-time research staff. He has published over 140 articles in the peer-reviewed literature pertaining to sea ice, climate change, and physical–biological coupling in the Arctic marine system.